JOURNAL OF APPLIED PHYSICS 116, 184903 (2014)

Experimental determination of the dynamics of an acoustically levitated sphere

Nicolás Pérez,[1,a)] Marco A. B. Andrade,[2] Rafael Canetti,[3] and Julio C. Adamowski[4]
[1]Centro Universitario de Paysandú, Universidad de la República, Paysandú, Uruguay
[2]Institute of Physics, University of São Paulo, São Paulo, Brazil
[3]Facultad de Ingeniería, Universidad de la República, Montevideo, Uruguay
[4]Department of Mechatronics and Mechanical Systems Engineering, Escola Politécnica, University of São Paulo, São Paulo, Brazil

(Received 12 August 2014; accepted 1 November 2014; published online 12 November 2014)

Levitation of solids and liquids by ultrasonic standing waves is a promising technique to manipulate materials without contact. When a small particle is introduced in certain areas of a standing wave field, the acoustic radiation force pushes the particle to the pressure node. This movement is followed by oscillations of the levitated particle. Aiming to investigate the particle oscillations in acoustic levitation, this paper presents the experimental and numerical characterization of the dynamic behavior of a levitated sphere. To obtain the experimental response, a small sphere is lifted by the acoustic radiation force. After the sphere lift, it presents a damped oscillatory behavior, which is recorded by a high speed camera. To model this behavior, a mass-spring-damper system is proposed. In this model, the acoustic radiation force that acts on the sphere is theoretically predicted by the Gor'kov theory and the viscous forces are modeled by two damping terms, one term proportional to the square of the velocity and another term proportional to the particle velocity. The proposed model was experimentally verified by using different values of sound pressure amplitude. The comparison between numerical and experimental results shows that the model can accurately describe the oscillatory behavior of the sphere in an acoustic levitator.
 [http://dx.doi.org/10.1063/1.4901579]

I. INTRODUCTION

Trapping, separation, and manipulation of small particles by ultrasonic standing waves have many potential applications in biology,[1–6] medicine,[7] analytical chemistry,[8,9] and in other fields.[10–14] Handling techniques by ultrasonic standing waves have been applied in many different studies, which include separation of lipids from blood,[7] measurement of surface tension of liquids,[13] and in the development of amorphous drugs.[15] Contrary to other noncontact manipulation techniques, such as magnetic levitation,[16] optical manipulation,[17] and electrostatic levitation,[18] acoustic handling techniques have the main advantage of not requiring any special property of the levitated particle.

The manipulation of particles by ultrasonic waves is possible due to the acoustic radiation force produced by a standing wave field,[19–21] which can act on particles immersed in liquids[2,4,22–24] and gases.[25–35] Depending on the density and the compressibility of the particle, and on the characteristics of the surrounding medium, the acoustic force can move the particle to a pressure node or to an antinode of a standing wave.[4] In the case of acoustic levitation in air, the acoustic radiation force normally moves the particle to a pressure node, because in most cases, the particle density is much higher than that of air and its compressibility is much lower than that of the surrounding fluid.[27]

Although it has been demonstrated that acoustic manipulation of particles can be performed in liquids and in the air, the manipulation in the air is more challenging, because the acoustic radiation force on the particle should be strong enough to counteract the gravity force. This contrasts with the manipulation of particles in liquids, in which the main contribution to the levitation is the buoyancy force. Recently, new acoustic devices have been proposed to suspend and to manipulate particles in the air.[25–29,36,37] With the manipulation systems proposed by Koyama and Nakamura, it is possible to transport particles in a linear[25] and in a circular trajectory.[26] The manipulation concept proposed by Foresti and coauthors allows the noncontact transportation and merging of liquid droplets in the air.[27] Another device proposed by the same authors was able to rotate particles and droplets in the air.[29]

In acoustic levitation experiments, samples of liquids and solids are normally inserted into the levitator by using tweezers and syringes. In order to fully explore the potential of acoustic levitation, an automatic system for sample deployment can increase the applicability of noncontact manipulation systems. For liquid samples, automatic drop dispensers have been used to insert droplets into the levitator.[9,38] In a single-axis acoustic levitator, consisting of an ultrasonic transducer and a reflector, a solid particle lying on the reflector can be lifted to the pressure node by just turning on the levitator. In both cases, liquid and solid samples oscillate around the equilibrium levitation position after they are inserted into the pressure node of the standing wave field. Oscillations of the levitated particle can also occur in

[a)]Author to whom correspondence should be addressed. Electronic mail: nico@fisica.edu.uy

noncontact manipulation devices, especially when the position of the pressure node is rapidly switched, causing the particle to jump from one position to another.[29,36] Oscillational instabilities of the levitated particle have also been reported,[39–42] possibly caused by acoustic streaming[43,44] and a time delay in the acoustic cavity response.[40]

The objective of this paper is to investigate the sample dynamics after it is inserted into the pressure node of an acoustic levitator. To study the sample dynamics, a small sphere is placed on the reflector of a single-axis acoustic levitator, and when the levitator is switched on, the acoustic radiation force pushes the sphere to the pressure node of the standing wave field. Immediately after the levitator is turned on, the sphere presents a damped oscillatory motion around the pressure node. This motion is recorded by a high speed camera and a tracking algorithm is used to obtain the sphere vertical position as a function of time. The sphere motion is analyzed by using the Finite Element Method and the Gor'kov theory,[20] which are applied to calculate the acoustic radiation force that acts on the sphere.

II. THEORY

The acoustic radiation force that acts on a small sphere in the presence of a standing wave field can be calculated by applying the Gor'kov theory.[20] According to this theory, the force **F** that acts on a rigid sphere of radius R is calculated by

$$\mathbf{F} = -\nabla U, \tag{1}$$

where U is the Gor'kov potential, given by[20,21]

$$U = 2\pi R^3 \left[\frac{\langle p^2 \rangle}{3\rho c^2} - \frac{\rho \langle u^2 \rangle}{2} \right], \tag{2}$$

where $\langle p^2 \rangle$ and $\langle u^2 \rangle$ are the mean square amplitudes of the sound pressure and velocity, respectively, ρ is the density of the fluid medium and c is the fluid sound velocity. The Gor'kov theory assumes that the sphere radius is much smaller than the wavelength λ.

In this paper, the acoustic radiation force is produced by a single-axis acoustic levitator consisting of a 20.34 kHz ultrasonic transducer with a concave radiating surface and a concave reflector. The complete description and the geometry of this levitator were previously presented[34] as well as its nonlinear characterization.[45] In order to predict the acoustic radiation force that acts on a sphere, a linear Finite Element Method (FEM) was used to simulate the acoustic pressure and velocity distributions in the air gap between the transducer and the reflector. Due to the large number of elements to ensure the convergence in a 3D simulation, the air gap was discretized with 2D axisymmetric elements with a mesh size of 0.2 mm, neglecting the influence of the groove on the acoustic radiation force. The simulation was performed by considering a sound velocity of 340 m/s and an air density of 1.2 kg/m^3. With the pressure and velocity distributions, the Gor'kov potential was calculated for a sphere of 3 mm diameter. The acoustic pressure amplitude and the Gor'kov potential are presented in Fig. 1. In the simulations, the Gor'kov potential was obtained for the levitator operating at 20 340 Hz with transducer displacement amplitude of 1 μm and separation distance of 28.6 mm between the transducer and the reflector. As the numerical model is linear, only one simulation is required to obtain the pressure distribution in the air gap between the transducer and the reflector. Although the pressure distribution of Fig. 1(a) was determined using a transducer displacement amplitude of 1 μm, it can be multiplied by a constant to find the pressure distribution for other displacement amplitudes. For a separation distance of 28.6 mm, a standing wave with three levitation positions is produced. These positions are denoted by the cross marks in Fig. 1. The levitation positions are located along the levitator main axis at 4.5, 14.2, and 24.0 mm from the bottom of the reflector. To find the spheres levitation positions, the gravity force was assumed to be small when compared to the acoustic forces. In this case, the particles are considered to be levitating at the positions of minimum acoustic potential, although, in practice, the equilibrium position is slightly below the positions of minimum Gor'kov potential due to the gravity force.

Figure 2 presents the Gor'kov potential along the z-axis. This figure also presents the vertical component of the acoustic radiation force that acts on the 3-mm sphere as a function of z. As can be observed in this figure, the acoustic radiation force is zero at the positions of minimum Gor'kov potential. It is also interesting to note that if the sphere is slightly

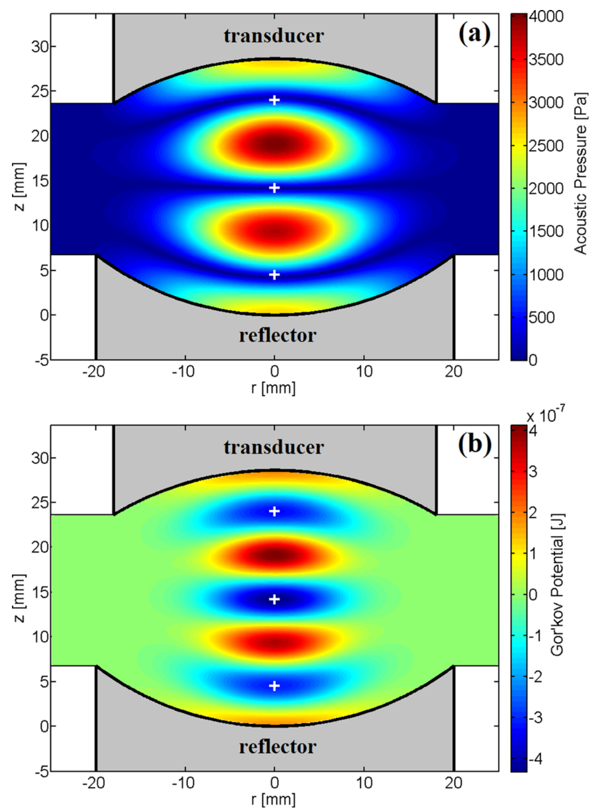

FIG. 1. (a) Simulated acoustic pressure and (b) Gor'kov potential calculated for a sphere of 3 mm diameter. In the simulation, the transducer face vibrates at 20 340 Hz with displacement amplitude of 1 μm and a separation distance of 28.6 mm was considered between the transducer and the reflector.

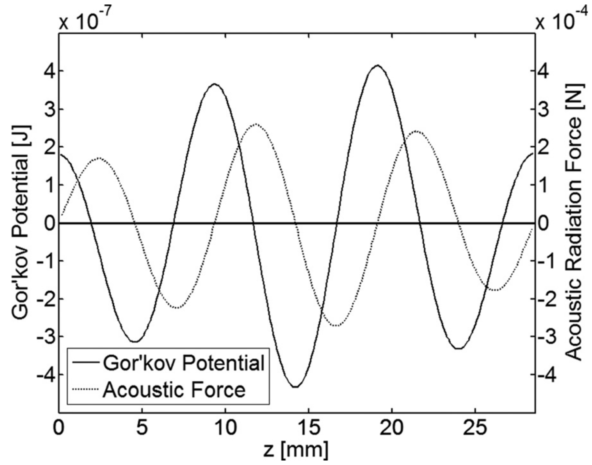

FIG. 2. Simulated Gor'kov Potential and the vertical component of the acoustic radiation force that acts on a 3-mm diameter sphere along the z-axis. The Gor'kov Potential and the acoustic radiation force were obtained for the same conditions of Fig. 1.

displaced from the minimum of the Gor'kov potential, the acoustic radiation force pushes the particle back to the equilibrium position. In the case of positions of maximum Gor'kov potential, the acoustic forces are also zero, but these positions are not used for levitation, because they correspond to unstable equilibrium states.

In the neighborhood of a minimum Gor'kov potential, the potential can be approximated by a parabola and the acoustic radiation force can be described by a linear restoring force (Hooke's law).[21,46] This allows to define an equivalent elastic constant for each equilibrium position, and as a consequence of Eq. (2), the equivalent elastic constant should have a quadratic dependence on the acoustic pressure amplitude.

In this paper, all levitation analysis is performed for the bottom equilibrium point located at $z = 4.5$ mm. By fitting a linear curve to the vertical acoustic radiation force of Fig. 2 in a neighborhood of $z = 4.5$ mm, it was obtained an equivalent elastic constant of 0.130 N/m. To relate the equivalent elastic constant with the pressure amplitude, a reference position should be specified. Here, the position of the second pressure antinode, located at $r = 0$, $z = 19.1$ mm, is defined as the reference position. The pressure amplitude at this point is denoted by P_2, and in the experiments, the pressure amplitude is measured in order to estimate the elastic constant of the bottom equilibrium point. The relationship between the elastic constant k and the pressure amplitude P_2 is obtained from the FEM simulation. By considering an elastic constant $k = 0.130$ N/m, a pressure amplitude P_2 of 4033 Pa, and assuming a quadratic dependence between k and P_2, we can express the elastic constant k as a function of P_2 by

$$k = (8 \times 10^{-9})P_2^2, \tag{3}$$

where the unit of k is N/m and P_2 is in Pa. As shown in Eq. (3), the elastic constant of the bottom levitation point can be calculated by using the pressure amplitude P_2 at the reference position $z = 19.1$ mm.

To study the particle dynamics, it is necessary to take into account the forces that act on the levitated object. Assuming a particle motion in the neighborhood of a minimum Gor'kov potential, the acoustic force can be modeled by a classic spring, with a restoring force proportional to the displacement from the equilibrium position. The other force acting on the mass is the viscous force, which can be described as a function of the sphere velocity. This function can be developed in powers of the velocity, and in the present case, the friction forces are represented by the first two terms of the power series, with a damping term proportional to the velocity and another term proportional to the square of the velocity. The Newton's equation for the levitated particle is then

$$m\frac{d^2z}{dt^2} = -b_2\frac{dz}{dt}\left|\frac{dz}{dt}\right| - b_1\frac{dz}{dt} - kz - mg, \tag{4}$$

where m is the mass of the particle, b_1 is the linear damping coefficient, b_2 is quadratic damping coefficient, and g is the gravitational acceleration. Recently, Foresti and Poulikakos[29] proposed a dynamic model similar to that described by Eq. (4) to predict the particle oscillations in a noncontact manipulation system. The main difference between the two models is that Eq. (4) includes a damping term proportional to the square of the velocity.

III. EXPERIMENTAL SETUP

The dynamic behavior of an acoustically levitated 3 mm diameter polypropylene sphere, of density 875 kg/m^3, is investigated with the experimental setup of Fig. 3. The levitator used in the experiments was described in a previous paper[34] and it basically consists of a 20.34 kHz Langevin ultrasonic transducer with a concave radiating surface, and a concave reflector. To facilitate the visualization of the sphere by the high-speed camera, a groove with a width of 5.0 mm and a depth of 5.6 mm was made on the surface of the reflector, as can be observed in Fig. 4. The distance between the transducer and the reflector is adjusted to approximately 28.6 mm, which results in three pressure nodes, as shown in Fig. 1. By comparing Fig. 1 with Fig. 4, the positions of minimum Gor'kov Potential can be observed to agree with the spheres levitation positions of Fig. 4. Due to the angle at which the picture was taken, the upper sphere cannot be seen in Fig. 4.

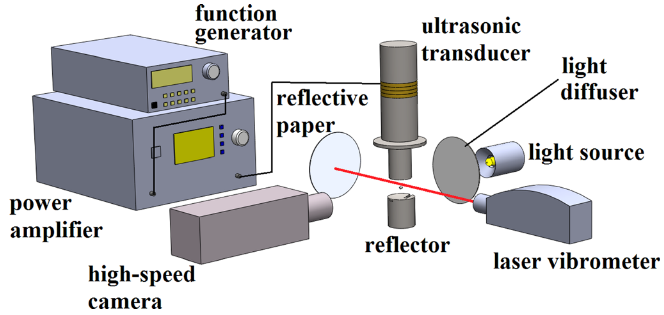

FIG. 3. Experimental setup.

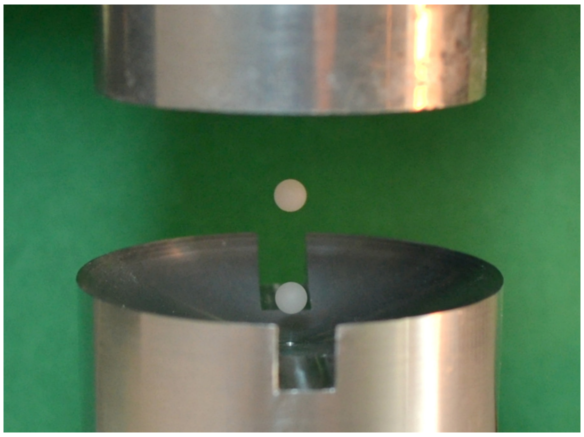

FIG. 4. Acoustic levitation of two polypropylene spheres at the pressure nodes of the single-axis acoustic levitator.

The ultrasonic transducer is driven by a function generator (33250A, Agilent Technologies Inc., Santa Clara, CA) connected to a power amplifier (800A3, Amplifier Research Corp., Souderton, PA). The function generator was programmed to produce a 20 340 Hz sine wave in bursts of 20 s, with 10 s on and 10 s off. In the experiments, the polypropylene sphere is placed on the reflector, and each time the output of the function generator is switched on, the acoustic radiation force pushes the sphere to the bottom pressure node ($z = 4.5$ mm) of the standing wave. After 10 s, the function generator is switched off and the sphere falls on the reflector. This cycle is recorded by a high-speed camera (Fastec Inline 1000, Fastec Imaging Corp., San Diego, CA). To synchronize the video recording with the function generator, the camera was triggered by the function generator. The dynamics of the polypropylene sphere was investigated by measuring the position of the sphere as a function of time for different values of acoustic pressure amplitude.

To investigate the dependence of the levitator elastic constant k with the pressure amplitude and to compare the experimental values of k with that predicted by Eq. (3), it is necessary to measure the sound pressure P_2 at ($r = 0$, $z = 19.1$ mm). Although the sound pressure can be measured by using a probe microphone,[47,48] it can disturb the sound field and change the acoustic radiation force on the sphere. To overcome this problem, the sound pressure amplitude P_2 at $z = 19.1$ mm is measured indirectly by using a Laser Doppler Vibrometer (LDV) (OFV-534 Sensor Head with an OFV-5000 controller, Polytec GmbH, Germany). The measurement of the sound pressure with a LDV is based on the change of the refractive index of air with the sound pressure.[25,49] Assuming a constant acoustic pressure amplitude P over the laser path and that the laser beam is reflected by a reflective surface, the LDV velocity output v_{LDV} can be calculated by[49]

$$v_{LDV} = \frac{2\pi f}{c^2 \rho} \frac{n-1}{n} PL, \tag{5}$$

where n is the refractive index of air, P is the pressure amplitude, f is the frequency, and L is the distance between the LDV sensor head and the reflective surface. However, it is clearly seen in Fig. 1(a) that the pressure amplitude varies with the radiation position. In this case, Eq. (5) is replaced by

$$v_{LDV} = \int \frac{2\pi f}{c^2 \rho} \frac{n-1}{n} P(r) dr, \tag{6}$$

and the integral is calculated over the laser path. To measure the pressure amplitude P_2, the LDV was positioned such that the laser beam passed through the point ($r = 0$, $z = 19.1$ mm). To convert the LDV velocity output v_{LDV} to pressure amplitude P_2, Eq. (6) was numerically integrated (from $r = -25$ mm to 25 mm, with $z = 19.1$ mm) by using the simulated pressure distribution of Fig. 1(a). At the laboratory conditions (0.92 atm, 20 °C) and for a laser wavelength of 633 nm, the refractive index of air corresponds to $n = 1.0002496$. From Eq. (6), a LDV velocity output of 15.3 mm/s was obtained. As this velocity output was calculated by considering a pressure amplitude $P_2 = 4033$ Pa and there was a linear relation between the pressure and the velocity output, the following relationship was obtained:

$$P_2[\text{Pa}] = 263594 v_{LDV}[\text{m/s}]. \tag{7}$$

This relation was used to obtain the experimental pressure amplitude P_2 from the vibrometer velocity measurements. To acquire the velocities signals, the vibrometer velocity output was connected to a 14-bit analog to digital converter (CS144002U, Gage Applied Technologies Inc., Lachine, Quebec, Canada). Due to the high intensity sound field in the air gap between the transducer and the reflector, the LDV signals contain harmonics of the fundamental frequency, which were caused by nonlinear propagation in the air.[45] The experimental value of P_2 was determined by calculating the Fast Fourier Transform (FFT) of the vibrometer signal and then taking the amplitude of the fundamental frequency of v_{LDV}, which was replaced in Eq. (7) to obtain P_2.

IV. RESULTS AND DISCUSSION

Using the experimental setup of Fig. 3, the step response of the levitating sphere is acquired by using different excitation levels. A typical sequence of frames obtained from the high-speed camera is presented in Fig. 5. This figure was obtained by setting the camera frame rate to 500 frames per second, and it shows the sphere position as a function of time immediately after the levitator is turned on. At the top left (frame A) of Fig. 5, the sphere is located at the bottom of the reflector. The subsequent frames clearly show an oscillatory motion of the sphere around the equilibrium levitation position. By applying a tracking algorithm, the position of the sphere was obtained as a function of time, as shown at the bottom right of Fig. 5.

In Fig. 5, the sphere is at rest at the bottom of the levitator (instant A). Then, the acoustic field is switched on and the sphere is pushed by the acoustic force to the maximum vertical position (instant B). The spheres oscillates around the equilibrium level (instants C, D, and E), and them the oscillations are damped due to the friction forces. A picture of the sphere at its equilibrium position is presented at the

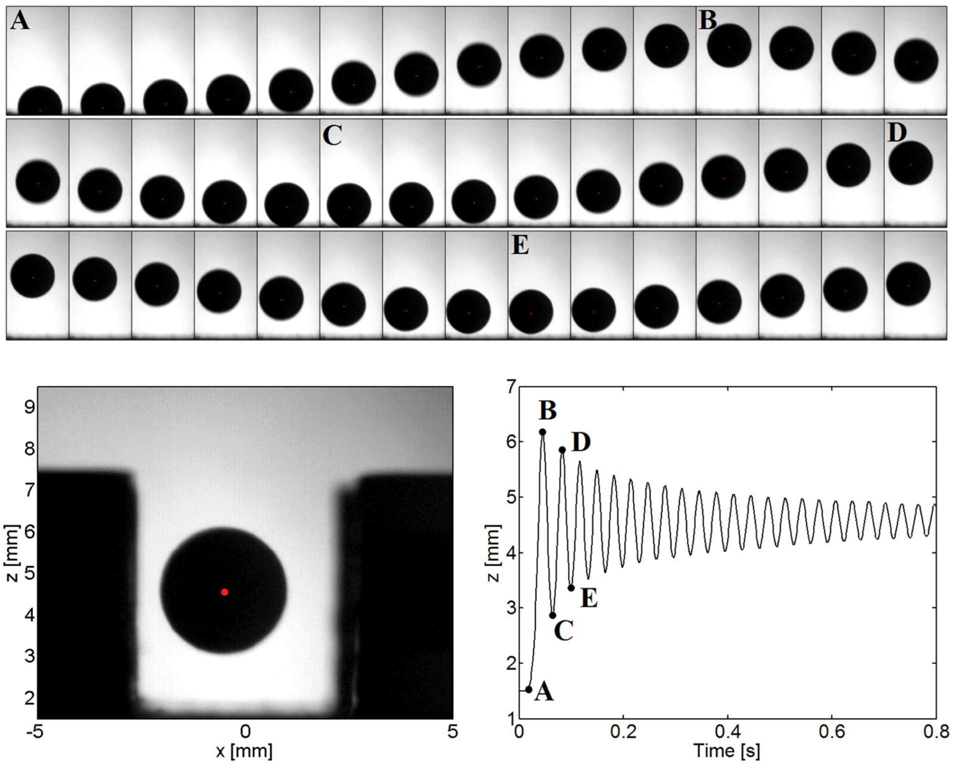

FIG. 5. The top figure presents a sequence of frames of a 3 mm polypropylene sphere obtained immediately after the acoustic levitator is turned on. The time between frames corresponds to 2 ms. The bottom left figure shows the picture of the levitating sphere at its equilibrium position, with the center dot representing its center of mass, and the bottom right figure shows the position of the sphere as a function of time. A video of the sphere position as a function of time is available online. (Multimedia view) [URL: http://dx.doi.org/10.1063/1.4901579.1]

bottom left of Fig. 5. This state is only perturbed by the fluctuations in the pressure field. In this experiment, the levitator was operating with a pressure amplitude P_2 of 8.1 kPa. This pressure amplitude was obtained indirectly by applying Eq. (7) to convert the LDV velocity output to P_2. For this pressure amplitude, the sphere oscillates with a resonance frequency of approximately 31 Hz around the equilibrium position.

In this paper, the position of the sphere as a function of time is modeled by using Eq. (4). This equation requires four parameters: the sphere mass m, and three additional parameters b_1, b_2, and k. The polypropylene sphere has a mass m of 12.2 mg, which was measured by an electronic balance. The other three parameters are adjusted to fit the experimental response. In order to obtain parameters b_1, b_2, and k, the adjustment is performed in a temporal window of 2.5 s, which starts from the first maximum of z. The coordinate system is translated such that the sphere equilibrium position corresponds to $z = 0$. Using this new coordinate system and starting from the maximum value of z, the response can be modeled as a mass-spring-damper system with initial conditions of zero velocity and finite displacement at $t = 0$. As the model proposed in Eq. (4) cannot be analytically solved, the differential equation is numerically integrated using a Runge-Kutta algorithm. The iterative procedure to find the parameters consists in minimizing three objective functions in parallel, each of them linked to a specific parameter. The elastic constant k is determined by calculating the FFT of the sphere position $z(t)$. Then, an optimization algorithm is used to find the value of k that minimizes the difference between the peaks of the numerical and the experimental FFT curves, as shown in Fig. 6. The objective functions to adjust b_1 and b_2 are the error in the energy of the signal in a predefined temporal window. For the parameter b_2, corresponding to the quadratic damping, the temporal window corresponds to the first 0.75 s. The temporal window for the linear damping coefficient b_1 was set to the last 0.75 s of the time interval. Figure 7 shows the result of the proposed model after the adjustment of the coefficients b_1, b_2, and k.

The comparison between the numerical and experimental sphere vertical position shows that the proposed model can predict the frequency of the sphere oscillations and the dependence of the oscillations amplitude with time. The sphere position obtained by the numerical model was determined by considering two damping parameters. In order to understand the influence of the damping parameters b_1 and b_2 on the damped oscillatory motion of the sphere, three different damping models are investigated. The first one ($b_1 > 0$, $b_2 = 0$) considers a damping force proportional to

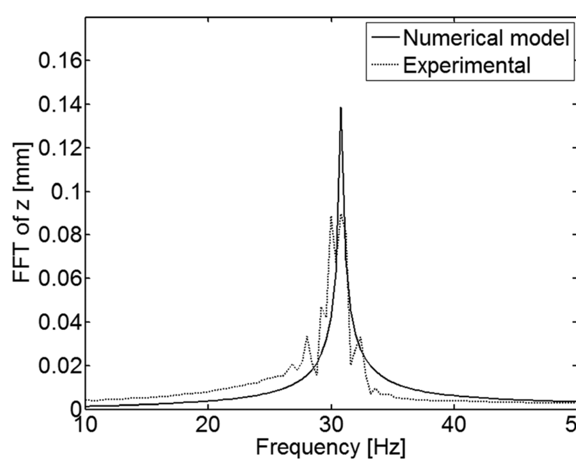

FIG. 6. Comparison between the experimental and numerical frequency spectrum of the vertical sphere position.

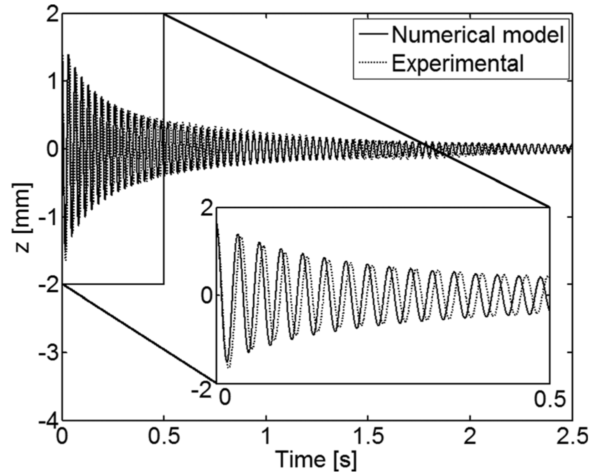

FIG. 7. Comparison between the sphere vertical position obtained experimentally and predicted by the proposed model after the parameters adjustment.

the velocity. In the second model ($b_1 = 0$, $b_2 > 0$), the damping force is proportional to the square of the velocity, and in the third model ($b_1 > 0$, $b_2 > 0$), the damping force is described as the linear combination of the two previous damping types. Figure 8 shows the influence of each damping model on the amplitude decay of the sphere oscillations. The experimental amplitude curve of Fig. 8 was determined by calculating the envelope of the vertical position of the sphere.

For a linear damping model ($b_1 > 0$, $b_2 = 0$), the motion equation can be solved analytically, resulting in an exponential decay of the oscillation amplitude. This exponential decay is represented by a straight line when plotted in a logarithmic scale. From the experimental amplitude curve of Fig. 8, one can observe that for times greater than 0.75 s, the logarithm of the amplitude decreases linearly with time. In this case, a linear damping model can describe the sphere damping. However, for times smaller than 0.75 s, the damping behavior is better described by a quadratic damping model ($b_1 = 0$, $b_2 > 0$). For the time interval between 0 and 2.5 s. two damping parameters ($b_1 > 0$, $b_2 > 0$) are necessary to describe the sphere damping behavior. In Fig. 8, the results of two linear damping models were presented. In the first linear model, it is imposed the same initial conditions as in the quadratic and two parameters model. In the second linear damping model, the initial conditions are arbitrary and only the amplitude decay at the final time interval is adjusted. From the results of Fig. 8, the Mean Square Error (MSE) between each numerical amplitude curve and the experimental curve was determined in the time interval between 0 and 2.5 s. It was obtained a MSE of 0.048 mm^2 for the first linear damping model, a MSE of 0.034 mm^2 for the second linear model, 0.0016 mm^2 for the quadratic damping model and 9.9×10^{-4} mm^2 for the two parameters damping model. The comparison between the three different damping models shows that only the two parameters damping model represents the sphere behavior in the time interval between 0 and 2.5 s.

Figure 9 presents the linear damping force and the quadratic damping force for the two parameters damping model. As can be observed in Fig. 9, few instants after the levitator is switched on, the quadratic damping is the mainly responsible for the sphere energy dissipation, and after 1.5 s, the linear damping has a major influence on the viscous forces. For times greater than 1.5 s, the oscillation behavior can be represented by a classical mass-spring-damper system, in which the viscous force is proportional to the particle velocity.

According to Eq. (2), the Gor'kov potential is proportional to the square of the acoustic pressure. Consequently, the elastic constant in the neighborhood of a point of a minimum potential is also proportional to the square of the pressure amplitude. For the particular case of the minimum potential located at $z = 4.5$ mm, it was found numerically that the elastic constant k can be calculated from the pressure amplitude P_2 by using Eq. (3). In order to verify this equation experimentally, the elastic constant k was obtained by using the adjustment procedure described previously. A total of 18 position curves $z(t)$ were considered in the adjustment procedure, with each curve being obtained for a different transducer excitation amplitude. The comparison between the numerical elastic constant obtained from Eq. (3) with

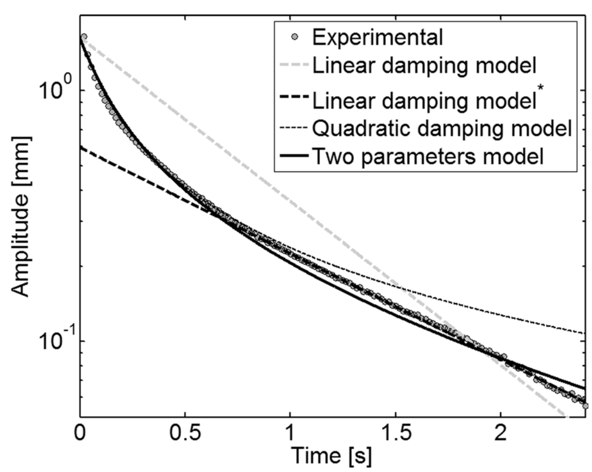

FIG. 8. Comparison between different damping models. In the first linear damping model, the b_1 coefficient was adjusted by considering an initial vertical position equal to 1.6 mm and in the second linear damping model, this condition was not imposed.

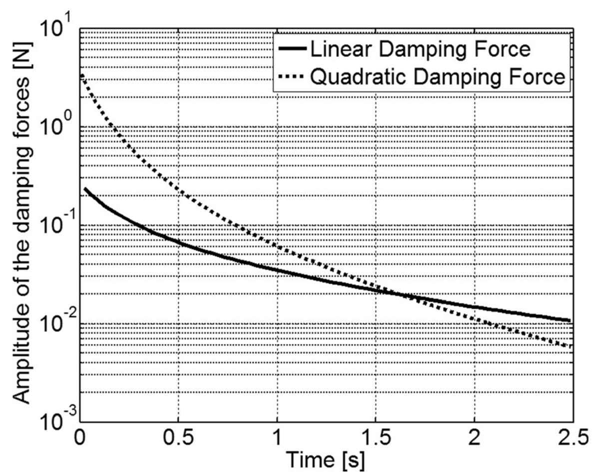

FIG. 9. Amplitude of the damping forces as a function of time.

that obtained experimentally from the adjustment procedure is presented in Fig. 10.

The numerical elastic constant k predicted by Eq. (3) can be used to determine the sphere oscillation frequency as a function of the pressure amplitude P_2. From the elastic constant k given by Eq. (3), the mass $m = 12.2$ mg of the polypropylene sphere, and assuming that the harmonic oscillator is lightly damped, the numerical oscillation frequency can be calculated by

$$f = \frac{1}{2\pi}\sqrt{\frac{k}{m}} = \left(4.07 \times 10^{-3}\right)P_2, \tag{8}$$

where f is in Hertz and P_2 is in Pa. A consequence of Eq. (8) is that the oscillation frequency of the sphere increases linearly with the pressure amplitude P_2. Another consequence is that the oscillation frequency goes to zero when the pressure amplitude is decreased to zero, although in practice the acoustic radiation force that acts on the sphere is not strong enough to keep the particle levitating for low values of pressure amplitude. The comparison between the numerical and experimental oscillation frequencies are presented in Fig. 11. This figure shows that there is a good agreement between numerical and experimental oscillation frequencies, especially for pressure amplitudes below 15 kPa. A possible cause for the differences that occurred above 15 kPa can be caused by the nonlinear effects.[50,51] When the levitator operates with high pressure amplitudes, part of the energy is transferred from the fundamental frequency to its harmonics, which can change the sound pressure distribution and the acoustic radiation force that acts on the particle.[45,52] As the numerical model used to obtain the acoustic radiation force is based on the linear acoustic theory, it cannot predict the influence of the harmonics on the oscillation frequency of the particle.

The particle oscillatory behavior described in this paper occurs not only when the particle is lifted from a surface, but also in a wide range of levitation experiments. The oscillations typically occur after inserting a small sample in the pressure node of the levitator. Recently, Chainani and coauthors[38] presented a new levitation setup in which a droplet launcher was used to insert small droplets into the levitator.

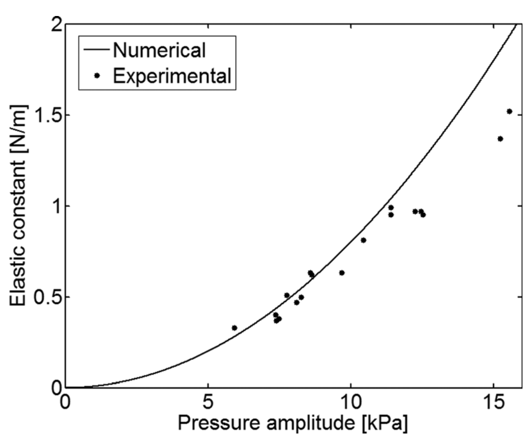

FIG. 10. Comparison between the numerical and experimental elastic constant k for the position of minimum acoustic potential located at the levitator main axis at $z = 4.5$ mm.

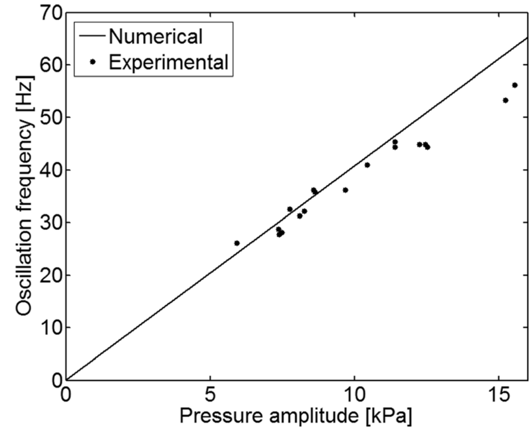

FIG. 11. Comparison between the numerical and experimental oscillation frequency of a polypropylene sphere of 3 mm diameter.

In a demonstration of their setup, a small droplet is levitating and another droplet is launched into the pressure node, which causes the collision with the levitating droplet. After the collision, the two droplets merge and the resulting droplet oscillates radially around the equilibrium position. In an interesting paper, Foresti and Poulikakos[29] presented a new acoustic manipulation device that is able to control the position of small particles in a circular trajectory. By controlling the amplitude of three different transducers, they could change the position of the minimum acoustic potential, and consequently, the particle is manipulated, because the particle follows the position of the minimum potential. In some conditions, the position of the minimum potential changes abruptly, which causes the particle to jump to the new minimum potential position. After the particle jumps, there is an oscillatory motion of the levitated particle, which is similar to the oscillatory motion described herein.

In this paper, it was investigated the damped oscillatory behavior of a solid sphere in a standing wave field. Although many potential applications of acoustic levitation require the levitation of liquid drops, it is simpler to analyze the dynamics of a solid sphere. When compared to a solid sphere, the dynamics of a levitating liquid drop is considerably more challenging to analyze, because there are many factors that can affect the dynamics of a levitating drop, such as the internal streaming[53] and the oscillations of the drop surface.[54]

Several papers have shown that the Gor'kov theory can accurately predict the levitation position of particles in acoustic levitators[30,34,39,55] and in noncontact manipulation systems.[27–29,35] The results presented in this paper shows that the Gor'kov theory can be used to describe the particles oscillations after it is inserted into the pressure node of an acoustic levitator.

V. CONCLUSIONS

This paper described the oscillatory behavior of a small sphere after it is lifted by the acoustic radiation force in a single-axis acoustic levitator. It was found that the oscillatory motion of the sphere, which occurs immediately after the detaching from the surface, can be described by a mass-spring-damper system. It was also verified that the viscous force that acts on the sphere should be described by two damping coefficients, one proportional to the particle velocity and the other proportional to the square of the velocity. Additionally, it was theoretically and experimentally shown that the acoustic radiation force that acts on the sphere in the neighborhood of a pressure node can be modeled by a spring, with an elastic constant proportional to the square of the pressure amplitude. A consequence of the quadratic dependence of the elastic constant on the pressure amplitude is that the particle oscillation frequency is proportional do the pressure amplitude. The comparison between the numerical and experimental oscillation frequencies shows that the Gor'kov theory could accurately predict the acoustic radiation force that acts on the polypropylene sphere. The indirect measurement of the sound pressure amplitude with a Laser Doppler Vibrometer was also presented. As the pressure amplitude is not constant over the laser path, the Finite Element Method was used to obtain a relation between the velocity output of the vibrometer with the acoustic pressure amplitude. The good agreement between the experimental and numerical oscillation frequencies not only shows that the Gor'kov theory can predict the acoustic radiation force on the particle, but also that the pressure amplitude can be accurately determined by using a Laser Doppler Vibrometer.

ACKNOWLEDGMENTS

We would like to thank the Brazilian funding agencies Petrobras/ANP, FAPESP, CNPq, and CAPES, and the Uruguayan funding agencies CSIC and ANII.

[1] L. Puskar, R. Tuckermann, T. Frosch, J. Popp, V. Ly, D. McNaughton, and B. R. Wood, Lab Chip **7**, 1125 (2007).
[2] N. Pamme, Lab Chip **7**, 1644 (2007).
[3] R. J. K. Weber, C. J. Benmore, S. K. Tumber, A. N. Tailor, C. A. Rey, L. S. Taylor, and S. R. Byrn, Eur. Biophys. J. **41**, 397 (2012).
[4] T. Laurell, F. Petersson, and A. Nilsson, Chem. Soc. Rev. **36**, 492 (2007).
[5] D. Hartono, Y. Liu, P. L. Tan, X. Y. S. Then, L. Y. L. Yung, and K. M. Lim, Lab Chip **11**, 4072 (2011).
[6] A. Scheeline and R. L. Behrens, Biophys. Chem. **165–166**, 1 (2012).
[7] F. Petersson, A. Nilsson, C. Holm, H. Jönsson, and T. Laurell, Analyst **129**, 938 (2004).
[8] S. Santesson, J. Johansson, L. S. Taylor, L. Levander, S. Fox, M. Sepaniak, and S. Nilsson, Anal. Chem. **75**, 2177 (2003).
[9] S. Santesson and S. Nilsson, "Airborne chemistry: Acoustic levitation in chemical analysis," Anal. Bioanal. Chem. **378**, 1704 (2004).
[10] J. Leiterer, F. Emmerling, U. Panne, W. Christen, and K. Rademann, Langmuir **24**, 7970 (2008).
[11] V. Vandaele, P. Lambert, and A. Delchambre, Precis. Eng. **29**, 491 (2005).
[12] V. Vandaele, A. Delchambre, and P. Lambert, J. Appl. Phys. **109**, 124901 (2011).
[13] Y. Tian, R. G. Holt, and R. E. Apfel, Rev. Sci. Instrum. **66**, 3349 (1995).
[14] J. R. Gao, C. D. Cao, and B. Wei, Adv. Space Res. **24**, 1293 (1999).
[15] C. J. Benmore and J. K. R. Weber, Phys. Rev. X **1**, 011004 (2011).
[16] A. K. Geim, M. D. Simon, M. I. Boamfa, and L. O. Heflinger, Nature **400**, 323–324 (1999).
[17] D. G. Grier, Nature **424**, 810 (2003).
[18] A. J. Rulison, J. L. Watkins, and B. Zambrano, Rev. Sci. Instrum. **68**, 2856 (1997).
[19] L. V. King, Proc. R. Soc. London, Ser. A **147**, 212 (1934).
[20] L. P. Gor'kov, Sov. Phys.-Dokl. **6**, 773 (1962).
[21] M. Barmatz and P. Collas, J. Acoust. Soc. Am. **77**, 928 (1985).
[22] X. Ding, S. C. S. Lin, B. Kiraly, H. Yue, S. Li, I. K. Chiang, J. Shi, S. J. Benkovic, and T. J. Huang, Proc. Natl. Acad. Sci. U.S.A. **109**, 11105 (2012).
[23] C. R. P. Courtney, C. E. M. Demore, H. Wu, A. Grinenko, P. D. Wilcox, S. Cochran, and B. W. Drinkwater, Appl. Phys. Lett. **104**, 154103 (2014).
[24] P. G. Glynne-Jones, C. E. M. Démoré, C. Ye, Y. Qiu, S. Cochran, and M. Hill, IEEE Trans. Ultrason. Ferroelectr. Freq. Control **59**, 1258 (2012).
[25] D. Koyama and K. Nakamura, IEEE Trans. Ultrason. Ferroelectr. Freq. Control **57**, 1152 (2010).
[26] D. Koyama and K. Nakamura, IEEE Trans. Ultrason. Ferroelectr. Freq. Control **57**, 1434 (2010).
[27] D. Foresti, M. Nabavi, M. Klingauf, A. Ferrari, and D. Poulikakos, Proc. Natl. Acad. Sci. U.S.A. **110**, 12549 (2013).
[28] D. Foresti, G. Sambatakakis, S. Bottan, and D. Poulikakos, Sci. Rep. **3**, 3176 (2013).
[29] D. Foresti and D. Poulikakos, Phys. Rev. Lett. **112**, 024301 (2014).
[30] W. J. Xie and B. Wei, Phys. Rev. E **66**, 026605 (2002).
[31] W. J. Xie, C. D. Cao, Y. J. Lü, Z. Y. Hong, and B. Wei, Appl. Phys. Lett. **89**, 214102 (2006).
[32] T. Kozuka, K. Yasui, T. Tuziuti, A. Towata, and Y. Iida, Jpn. J. Appl. Phys., Part 1 **47**, 4336 (2008).
[33] F. Priego-Capote and L. Castro, Trends Anal. Chem **25**, 856 (2006).
[34] M. A. B. Andrade, F. Buiochi, and J. C. Adamowski, IEEE Trans. Ultrason. Ferroelectr. Freq. Control **57**, 469 (2010).
[35] M. A. B. Andrade, N. Pérez, F. Buiochi, and J. C. Adamowski, IEEE Trans. Ultrason. Ferroelectr. Freq. Control **58**, 1674 (2011).
[36] S. A. Seah, B. W. Drinkwater, T. Carter, R. Malkin, and S. Subramanian, IEEE Trans. Ultrason. Ferroelectr. Freq. Control **61**, 1233 (2014).
[37] T. Hoshi, Y. Oachi, and J. Rekimoto, Jpn. J. Appl. Phys., Part 1 **53**, 07KE07 (2014).
[38] E. T. Chainani, W. H. Choi, K. T. Ngo, and A. Scheeline, Anal. Chem. **86**, 2229 (2014).
[39] S. Baer, M. A. B. Andrade, C. Esen, J. C. Adamowski, G. Schweiger, and A. Ostendorf, Rev. Sci. Instrum. **82**, 105111 (2011).
[40] J. Rudnick and M. Barmatz, J. Acoust. Soc. Am. **87**, 81 (1990).
[41] A. Santillan, in *Proceedings of the IEEE Ultrasonics Symposium* (2011), p. 1552.
[42] M. A. B. Andrade, N. Pérez, and J. C. Adamowski, J. Acoust. Soc. Am. **136**, 1518 (2014).
[43] E. H. Trinh and J. L. Robey, Phys. Fluids **6**, 3567 (1994).
[44] K. Hasegawa, Y. Abe, A. Kaneko, Y. Yamamoto, and K. Aoki, Microgravity Sci. Technol. **21**, 9 (2009).
[45] M. A. B. Andrade, T. S. Ramos, F. T. A. Okina, and J. C. Adamowski, Rev. Sci. Instrum. **85**, 045125 (2014).
[46] E. H. Trinh and C. J. Hsu, J. Acoust. Soc. Am. **80**, 1757 (1986).
[47] Y. Abe, D. Hyuga, S. Yamada, and K. Aoki, Ann. N.Y. Acad. Sci. **1077**, 49 (2006).
[48] A. Stindt, M. A. B. Andrade, M. Albrecht, J. C. Adamowski, U. Panne, and J. Riedel, Rev. Sci. Instrum. **85**, 015110 (2014).
[49] K. Nakamura, in *Proceedings of the 4th Pacific Rim Conference on Lasers and Electro-Optics* (IEEE, 2001), Vol. 1, p. 154.
[50] Y. A. Ilinskii, B. Lipkens, T. S. Lucas, T. W. Van Doren, and E. Z. Zabolotskaya, J. Acoust. Soc. Am. **104**, 2664 (1998).
[51] C. C. Lawrenson, B. Lipkens, T. S. Lucas, D. K. Perkins, and T. W. Van Doren, J. Acoust. Soc. Am. **104**, 623 (1998).
[52] E. Leung, N. Jacobi, and T. Wang, J. Acoust. Soc. Am. **70**, 1762 (1981).
[53] C. L. Shen, W. J. Xie, Z. L. Yan, and B. Wei, Phys. Lett. A **374**, 4045 (2010).
[54] C. L. Shen, W. J. Xie, and B. Wei, Phys. Rev. E **81**, 046305 (2010).
[55] W. J. Xie and B. Wei, Appl. Phys. Lett. **79**, 881 (2001).